

Generative Adversarial Super-Resolution at the edge with knowledge distillation

Original

Generative Adversarial Super-Resolution at the edge with knowledge distillation / Angarano, Simone; Salvetti, Francesco; Martini, Mauro; Chiaberge, Marcello. - In: ENGINEERING APPLICATIONS OF ARTIFICIAL INTELLIGENCE. - ISSN 0952-1976. - STAMPA. - 123 B:(2023). [10.1016/j.engappai.2023.106407]

Availability:

This version is available at: 11583/2978468 since: 2023-06-07T09:25:29Z

Publisher:

Elsevier

Published

DOI:10.1016/j.engappai.2023.106407

Terms of use:

This article is made available under terms and conditions as specified in the corresponding bibliographic description in the repository

Publisher copyright

(Article begins on next page)



Generative Adversarial Super-Resolution at the edge with knowledge distillation

Simone Angarano^{a,b,*}, Francesco Salvetti^{a,b,c}, Mauro Martini^{a,b}, Marcello Chiaberge^{a,b}

^a Politecnico di Torino, Corso Duca degli Abruzzi 24, Torino, 10129, Italy

^b PIC4SeR - PoliTo Interdepartmental Center for Service Robotics, Corso Ferrucci 112, Torino, 10141, Italy

^c SmartData@PoliTo, Corso Ferrucci 112, Torino, 10141, Italy

ARTICLE INFO

Keywords:

Super-Resolution
Edge-AI
Knowledge distillation
Real-time systems
GAN
Robotics

ABSTRACT

Single-Image Super-Resolution can support robotic tasks in environments where a reliable visual stream is required to monitor the mission, handle teleoperation or study relevant visual details. In this work, we propose an efficient Generative Adversarial Network model for real-time Super-Resolution, called EdgeSRGAN¹. We adopt a tailored architecture of the original SRGAN and model quantization to boost the execution on CPU and Edge TPU devices, achieving up to 200 fps inference. We further optimize our model by distilling its knowledge to a smaller version of the network and obtain remarkable improvements compared to the standard training approach. Our experiments show that our fast and lightweight model preserves considerably satisfying image quality compared to heavier state-of-the-art models. Finally, we conduct experiments on image transmission with bandwidth degradation to highlight the advantages of the proposed system for mobile robotic applications.

1. Introduction

In the last decade, Deep Learning (DL) techniques have pervaded robotic systems and applications, drastically boosting automation in both perception (de Queiroz Mendes et al., 2021; Zhu et al., 2021), navigation and control (Roy and Chowdhury, 2021; Xiao et al., 2022) tasks. The development of Machine Learning driven algorithms is paving the way for advanced levels of autonomy for mobile robots, widely increasing the reliability of both unmanned aerial vehicles (UAV) and unmanned ground vehicles (UGV) (de Queiroz Mendes et al., 2021). Nonetheless, the adoption of mobile robots for mapping and exploration (Lluvia et al., 2021), search and rescue (Drew, 2021) or inspection (Yuan et al., 2022; Yin, 2021) missions in harsh unseen environments can provide substantial advantages and reduce the risks for human operators. In this context, the successful transmission of images acquired by the robot to the ground station often assumes a significant relevance to the task at hand, allowing the human operators to get real-time information, monitor the state of the mission, take critical planning decisions and analyze the scenario. Moreover, unknown outdoor environments may present unexpected extreme characteristics which still hinder the release of unmanned mobile robots in the complete absence of human supervision. Although novel DL-based autonomous navigation algorithms are currently under investigation in disparate outdoor contexts such as tunnel exploration (Rouček et al.,

2019; Tardioli et al., 2019; Elmokadem and Savkin, 2022), row-crops navigation (Martini et al., 2022; Aghi et al., 2021) and underwater (Li et al., 2021; Almanza-Medina et al., 2021), complete or partial remote teleoperation remains the most reliable control strategy in uncertain scenarios. Indeed, irregular terrain, lighting conditions, and the loss of localization signal can lead navigation algorithms to fail. As a direct consequence of navigation errors, the robotic platform can get stuck in critical states where human intervention is required or preferred.

However, visual data transmission for robot teleoperation, monitoring, or online data processing requires a stable continuous stream of images, which may be drastically affected by poor bandwidth conditions due to the long distance of the robot or by constitutive factors of the specific environment. Besides this, UAVs and high-speed platforms require the pilot to receive the image stream at a high framerate to follow the vehicle's motion in non-line-of-sight situations. A straightforward but effective solution to mitigate poor bandwidth conditions and meet high-frequency transmission requirements is reducing the transmitted image's resolution. On the other hand, heavy image compression with massive loss of detail can compromise image usability.

To this end, we propose EdgeSRGAN, a novel deep learning model for Single-Image Super-Resolution (SISR) at the edge to handle the problem of efficient image transmission. Our intuition relies on a lightweight neural network allowing us to send low-resolution images at a high transmission rate with scarce bandwidth and then reconstruct

* Correspondence to: PIC4SeR, Corso Ferrucci 112, Torino, 10141, Italy.

E-mail addresses: simone.angarano@polito.it (S. Angarano), francesco.salvetti@polito.it (F. Salvetti), mauro.martini@polito.it (M. Martini), marcello.chiaberge@polito.it (M. Chiaberge).

¹ Code available at <https://github.com/PIC4SeR/EdgeSRGAN>.

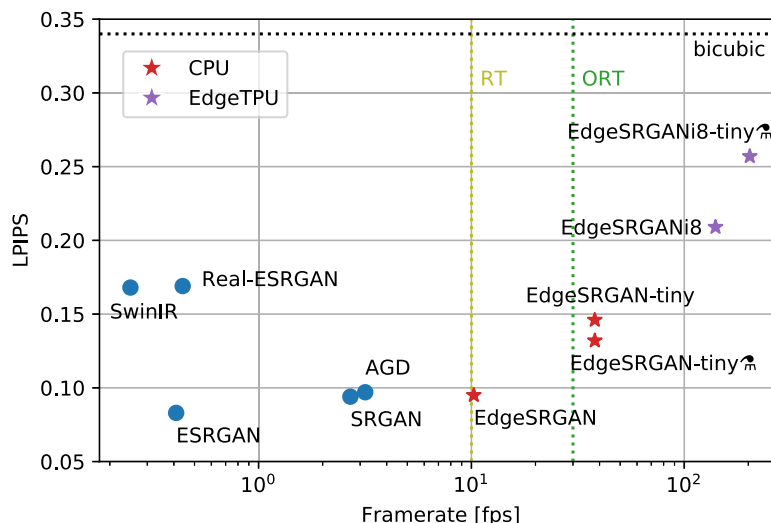


Fig. 1. LPIPS (Zhang et al., 2018a) results (lower is better) on Set5 (Bevilacqua et al., 2012) vs. framerate (80 × 60 input) of different visual-oriented SISR methods for ×4 upsampling. Real-time (RT) and over-real-time (ORT) framerates are marked as references. Our models, marked with *, reach real-time performance with a competitive perceptual similarity index on the CPU. Edge TPU models can further increase inference speed far beyond real-time, still outperforming the bicubic baseline.

the high-resolution image on the pilot’s mobile device. Moreover, the successful spread of edge-AI in different engineering applications (Chen and Ran, 2019; Angarano et al., 2021; Liu et al., 2021) has shown encouraging results in moving the execution of DL models on ultra-low power embedded devices. Hence, we propose an edge-AI computationally efficient Super Resolution neural network to provide fast inference on CPUs and Edge TPU devices. To this aim, we adopt several optimization steps to boost the performance of our model while minimizing the quality drop. We refine the architecture of the original SRGAN (Ledig et al., 2017) to speed up inference and perform model quantization. Nonetheless, we experiment with a teacher–student knowledge distillation technique for SISR to further enhance the reconstructed image of our tiny model. We take inspiration from the work of He et al. (2020) and obtain a remarkable improvement for all the considered metrics.

We perform experiments to validate the proposed methodology under multiple perspectives: numerical and qualitative analysis of our model reconstructed images and inference efficiency on both CPU and Edge TPU devices. As an example, as shown in Fig. 1, EdgeSRGAN achieves real-time performance with a competitive perceptual similarity index compared with other visual-oriented SISR methods. Moreover, we test the performance of our system for robotic applications. In particular, we focus on image transmission for teleoperation in case of bandwidth degradation, also performing tests with the popular robotic middleware ROS2.

The rest of the paper is organized as follows. In Section 2, we introduce the research landscape of Super-Resolution (SR), starting from the general background and then deepening the discussion towards robotic applications of SR and efficient SR methods presented in previous works. In Section 3, we describe the Super-Resolution problem and our methodological steps to obtain an Edge AI implementation for real-time performances. In Section 4, we propose a wide range of experiments to validate the proposed methodology, analyzing the results obtained for inference speed and output image quality and characterizing the advantages of our approach for robotic applications in limited-bandwidth conditions. Finally, in Section 5, we summarize the overall study with conclusive remarks and suggest some potential future work directions.

2. Related works

2.1. Single-image super-resolution

Single-Image Super-Resolution, also referred to as super-sampling or image restoration, aims at reconstructing a high-resolution (HR)

image starting from a single low-resolution (LR) input image, trying to preserve details and the information conceived by the image. Therefore SISR, together with image denoising, is an ill-posed underdetermined inverse problem since a multiplicity of possible solutions exist given an input low-resolution image. Recently, learning-based methods have rapidly reached state-of-the-art performance and are universally recognized as the most popular approach for Super-Resolution. Such approaches rely on learning common patterns from multiple LR-HR pairs in a supervised fashion. SRCNN (Dong et al., 2015) was the first example of a CNN applied to single-image super-resolution in literature. It has been followed by multiple methods applying standard deep learning methodologies to SISR, such as residual learning (Kim et al., 2016; Lim et al., 2017), dense connections (Zhang et al., 2018c), residual feature distillation (Liu et al., 2020), attention (Zhang et al., 2018b; Dai et al., 2019; Niu et al., 2020), self-attention, and transformers (Cao et al., 2021; Chen et al., 2021; Liang et al., 2021). All these works focus on content-based SR, in which the objective is to reconstruct an image with high pixel fidelity, and the training is based on a content loss, such as mean square error or mean absolute error.

In parallel, other works proposed Generative Adversarial Networks (GAN) (Goodfellow et al., 2014) for SISR to aim at reconstructing visually pleasing images. In this case, the focus is not on pixel values but perceptual indexes that try to reflect how humans perceive image quality. This is usually implemented using perceptual losses and adversarial training and is referred to as visual-based SR. SRGAN (Ledig et al., 2017) first proposed adversarial training and was later followed by other works (Lim et al., 2017; Fu et al., 2020; Wang et al., 2021a). With robotic image transmission as a target application in mind, in this work, we particularly focus on visual-based SR, aiming to reconstruct visually pleasing images to be used by human operators for real-time teleoperation and monitoring.

2.2. Efficient methods for single-image super-resolution

In recent years, efficient deep neural networks for SR have been proposed to reduce the number of parameters while keeping high-quality performances (Li et al., 2022). However, most of the proposed architectural solutions are designed for content-based training, which aims to minimize the difference between the high-resolution image and the network output. Among them, Sajjadi et al. (2017) proposed a thin, simple model which handles SR as a bilinear upsampling residual compensation. Despite the high-quality images obtained, this approach has high inference latency due to the double prediction required.

Diversely, [Michelini et al. \(2022\)](#) entirely based their study to target Edge-AI chips, proposing an ultra-tiny model composed of one layer only.

As already stated, we prefer GAN-based SR to enhance the visual appearance of produced images for robotic applications. However, successful studies of efficient GANs are very rare in the literature. Recently, knowledge distillation (KD) emerged as a promising option to compress deep models and GANs too ([Aguinaldo et al., 2019](#); [Gou et al., 2021](#)). KD was originally born in 2015 with the visionary work of [Hinton et al. \(2015\)](#), where a teacher–student framework was introduced as a knowledge transfer mechanism. More recent works evolved such concept in disparate variants: FitNet introduced the idea of involving also intermediate representations in the distillation process ([Romero et al., 2014](#)), AT proposes an attention-based distillation ([Zagoruyko and Komodakis, 2016](#)), and AB interestingly focuses on the distilled transfer of activation boundaries formed by hidden neurons ([Heo et al., 2019b](#)), further advanced in [Heo et al. \(2019a\)](#). Specifically considering KD application in SR, FAKD uses intermediate features affinity distillation for PSNR-focused SR ([He et al., 2020](#)). We found this approach a good starting point also for GAN-based SR. Diversely, [Zhang et al. \(2021\)](#) investigates a progressive knowledge distillation method for data-free training. Besides KD, [Fu et al. \(2020\)](#) recently proposed an Auto-ML framework to search for optimal neural model structure, and filter pruning has been used as another optimization technique ([Li et al., 2017](#)).

Differently from previous works, our model optimization for edge-SR is composed of three main steps: first, an edge-oriented architectural definition is performed; then, we leverage teacher–student knowledge distillation to further reduce the dimension of our model; lastly, we perform TFLite conversion and quantization to shift the network execution to CPUs and Edge TPUs with maximum inference speed.

2.3. Super-resolution for robotic applications

SISR has been recently proposed in a few robotic applications where a high level of detail is beneficial to support the specific task. Research on the indoor teleoperation of mobile robots mainly focuses on improving user experience, combining Deep Learning methods with Virtual Reality ([Zein et al., 2021](#); [Hedayati et al., 2018](#); [Stotko et al., 2019](#)), but neglecting the potential bottleneck caused by connectivity degradation in harsh conditions. Differently, a great effort has been devoted to SISR for underwater robotics perception ([Ooyama et al., 2021](#); [Islam et al., 2020](#)), effectively tackling the problem of high-quality image acquisition under the sea for accurate object and species detection. Besides autonomous navigation applications, interesting contexts are robotic surgery ([Wang et al., 2021b](#); [Brodie and Vasdev, 2018](#)) and medical robots research ([Martinez et al., 2021](#)), where SISR can provide substantial advantages improving the visibility and increasing the level of detail required for delicate high-precision movements of the surgeon. Similarly, a detailed image acquired by a robot is needed for monitoring and inspection purposes. For example, [Bae et al. \(2021\)](#) uses a Super-Resolution model to enhance the online crack detection and in-situ analysis of bridge weaknesses. Nonetheless, no relevant works proposed so far have identified Super-Resolution as an efficient solution for image transmission to support robot teleoperation and exploration of unknown environments in bandwidth-degraded conditions.

3. Methodology

In this section, we introduce all the components of the proposed methodology. As explained in Section 1, we choose to use an adversarial approach to obtain an optimal balance between pixel-wise fidelity and perceptual quality. For this reason, we take inspiration from three of the most popular GAN-based solutions for SISR: SRGAN ([Ledig et al., 2017](#)), ESRGAN ([Wang et al., 2018b](#)), and AGD ([Fu et al., 2020](#)). The proposed method aims to obtain a real-time SISR model

(EdgeSRGAN) with minimal performance drop compared to state-of-the-art solutions. For this reason, we mix successful literature practices with computationally-efficient elements to obtain a lightweight architecture. Then, we design the network training procedure to leverage a combination of pixel-wise loss, perceptual loss, and adversarial loss. To further optimize the inference time, we apply knowledge distillation to transfer the performance of EdgeSRGAN to an even smaller model (EdgeSRGAN-tiny). Furthermore, we study the effect of quantization on the network's latency and accuracy. Finally, we propose an additional inference-time network interpolation feature to allow real-time balancing between pixel-wise precision and photo-realistic textures.

3.1. Network architecture

As previously done by [Wang et al. \(2018b\)](#), we take the original design of SRGAN and propose some changes to both the architecture and training procedure. However, in our case, the modifications seek efficiency as well as performance. To obtain a lighter architecture, we reduce the depth of the model by using only $N = 8$ Residual Blocks instead of the original 16. In particular, we use simple residuals instead of the Residual-in-Residual Dense Blocks (RRDB) proposed by [Wang et al. \(2018b\)](#) as they are less computationally demanding. For the same reason, we change PReLU activation functions into basic ReLU. We also remove Batch Normalization to allow the model for better convergence without generating artifacts ([Wang et al., 2018b](#)). Finally, we use Transpose Convolution for the upsampling head instead of Sub-pixel Convolution ([Shi et al., 2016](#)). Despite its popularity and effectiveness, Sub-pixel Convolution is computationally demanding due to the Pixel Shuffling operation, which rearranges feature channels spatially. We choose instead to trade some performance for efficiency and apply Transpose Convolutions taking precautions to avoid problems such as checkerboard artifacts ([Odena et al., 2016](#)). The complete EdgeSRGAN architecture is described in [Fig. 2](#). The adopted discriminator model is the same used in [Ledig et al. \(2017\)](#) and [Wang et al. \(2018b\)](#), as it serves only training purposes and is not needed at inference time. Its architecture is described in [Fig. 3](#).

3.2. Training methodology

The training procedure is divided into two sections, as it is common practice in generative adversarial SISR. The first part consists of classic supervised training using pixel-wise loss. In this way, we help the generator to avoid local minima and generate visually pleasing results in the subsequent adversarial training. We use the mean absolute error (MAE) loss for the optimization as it has recently proven to bring better convergence than mean squared error (MSE) ([Zhao et al., 2016](#); [Lim et al., 2017](#); [Zhang et al., 2018b](#); [Wang et al., 2018b](#)).

$$L_{\text{MSE}} = \sum_{i=1}^B \|y_i^{\text{HR}} - y_i^{\text{SR}}\|_1 \quad (1)$$

where y^{HR} is the ground-truth high resolution image, y^{SR} is the output of the generator, and B is the batch size. We use the Peak Signal-to-Noise Ratio (PSNR) metric to validate the model.

In the second phase, the resulting model is fine-tuned in an adversarial fashion, optimizing a loss that takes into account adversarial loss and perceptual loss. As presented in [Ledig et al. \(2017\)](#), the generator G training loss can be formulated as

$$L_G = L_G^P + \xi L_G^A + \eta L_{\text{MSE}}. \quad (2)$$

L_G^P is the perceptual VGG54 as the euclidean distance between the feature representations of a reconstructed image SR and the reference image HR. The features are extracted using the VGG19 network ([Simonyan and Zisserman, 2015](#)) pre-trained on ImageNet:

$$L_G^P = \sum_{i=1}^B \|\phi(y_i^{\text{HR}}) - \phi(y_i^{\text{SR}})\|_2 \quad (3)$$

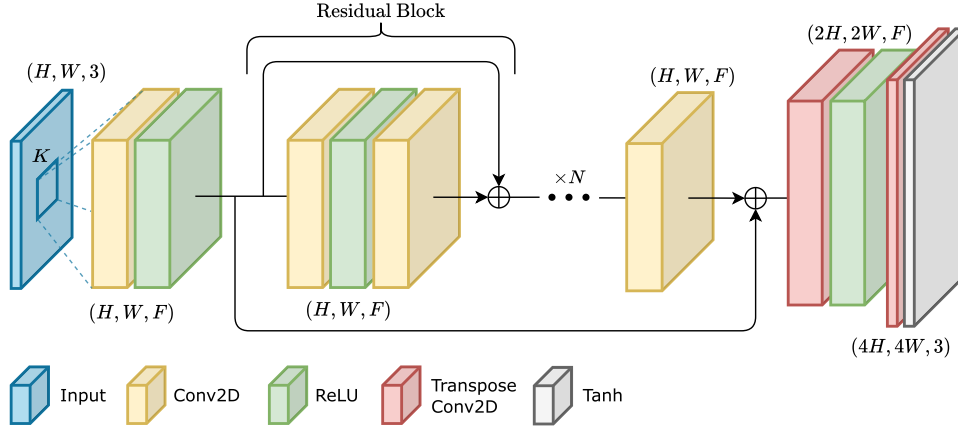


Fig. 2. EdgeSRGAN generator architecture.

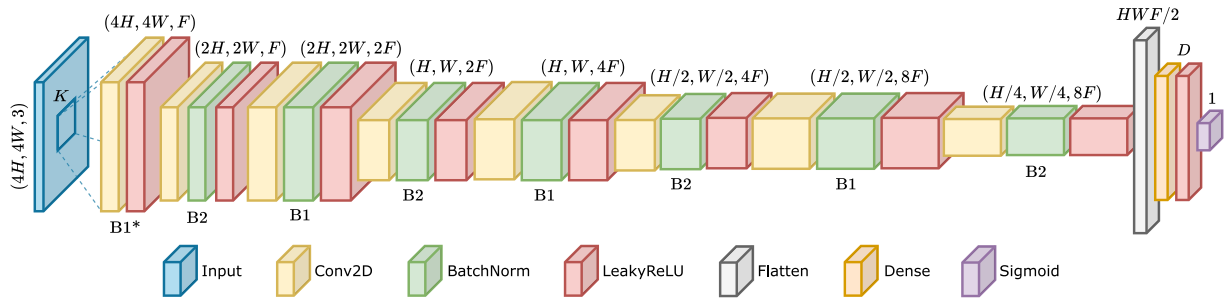


Fig. 3. EdgeSRGAN discriminator architecture. The model progressively reduces the spatial dimensions of the image by alternating blocks with strides 1 (B1) and 2 (B2). The first block (marked with *) does not apply batch normalization.

where ϕ is the perceptual model VGG. L_G^A is the adversarial generator loss, defined as

$$L_G^A = -\log(D(y_{SR})) \quad (4)$$

where D is the discriminator. Using this loss, the generator tries to fool the discriminator by generating images that are indistinguishable from the real HR ones. ξ and η are used to balance the weight of different loss components. The weights of the discriminator D are optimized using a symmetrical adversarial loss, which tends to correctly discriminate HR and SR images.

$$L_D = \log(D(y_{SR})) - \log(D(y_{HR})) \quad (5)$$

We optimize both models simultaneously, without alternating weight updates like in most seminal works on GANs. The overall training methodology is summarized in Fig. 4 summarizes the overall training methodology.

3.3. Knowledge distillation

As mentioned in Section 2, Knowledge Distillation (KD) has gained increasing interest in deep learning for its ability to transfer knowledge from bigger models to simpler ones efficiently. In particular, KD has been applied in some SISR works to compress the texture reconstruction capability of cumbersome models and obtain efficient real-time networks. However, to the best of our knowledge, KD has never been applied to GAN SISR models. For this reason, we adapt an existing technique developed for SISR called Feature Affinity-based Knowledge Distillation (FAKD) (He et al., 2020) to the GAN training approach. The FAKD methodology transfers second-order statistical info to the student by aligning feature affinity matrices at different layers of the networks. This constraint helps to tackle the fact that regression problems generate unbounded solution spaces. Indeed, most of the KD methods so far

have only tackled classification tasks. Given a layer l of the network, the feature map F_l extracted from that layer (after the activation function) has the following shape:

$$F_l \in \mathbb{R}^{B \times C \times W \times H} \quad (6)$$

where B is the batch size, C is the number of channels, W and H are the width and the height of the tensor. We first flatten the tensor along the last two components obtaining the three-dimensional feature map

$$F_l \in \mathbb{R}^{B \times C \times WH} \quad (7)$$

which now holds all the spatial information along a single axis. We define the affinity matrix A_l as the product

$$A_l = \tilde{F}_l^T \cdot \tilde{F}_l \quad (8)$$

where \cdot is the matrix multiplication operator and the transposition T swaps the last two dimensions of the tensor. \tilde{F}_l is the normalized feature map, obtained as

$$\tilde{F}_l = \frac{F_l}{\|F_l\|_2} \quad (9)$$

Differently from He et al. (2020), the norm is calculated for the whole tensor and not only along the channel axis. Moreover, we find better convergence using the euclidean norm instead of its square. In this way, the affinity matrix has a shape

$$A_l \in \mathbb{R}^{B \times WH \times WH} \quad (10)$$

and the total distillation loss L_{Dist} becomes

$$L_{Dist} = \frac{1}{N_L} \left(\sum_{l=1}^{N_L} \|A_l^T - A_l^S\|_1 \right) + \lambda \|y_{SR}^T - y_{SR}^S\|_1 \quad (11)$$

where N_L is the number of distilled layers. Differently from He et al. (2020), we sum the loss along all the tensor dimensions and average the

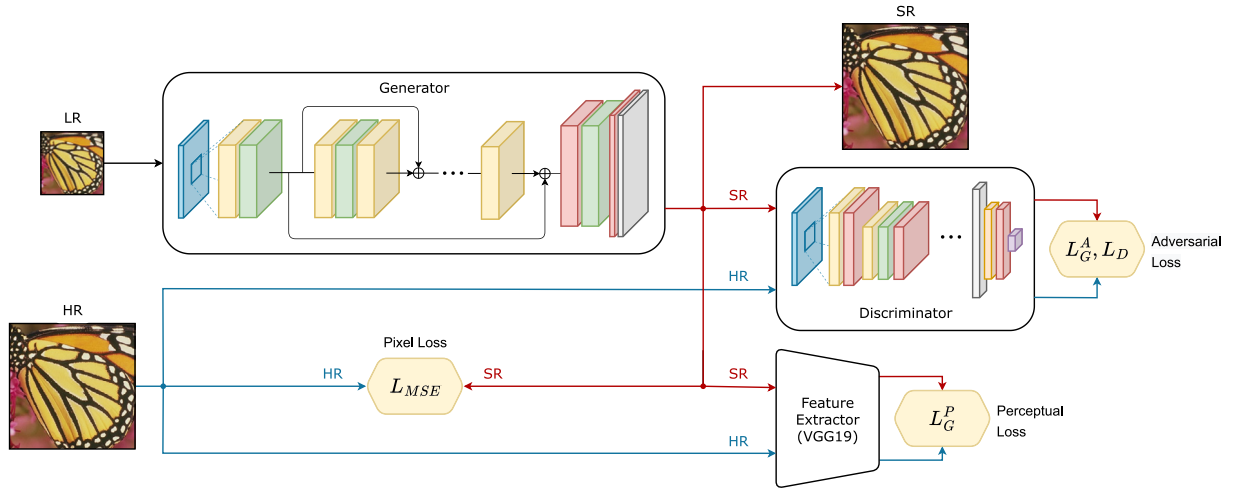


Fig. 4. EdgeSRGAN training methodology.

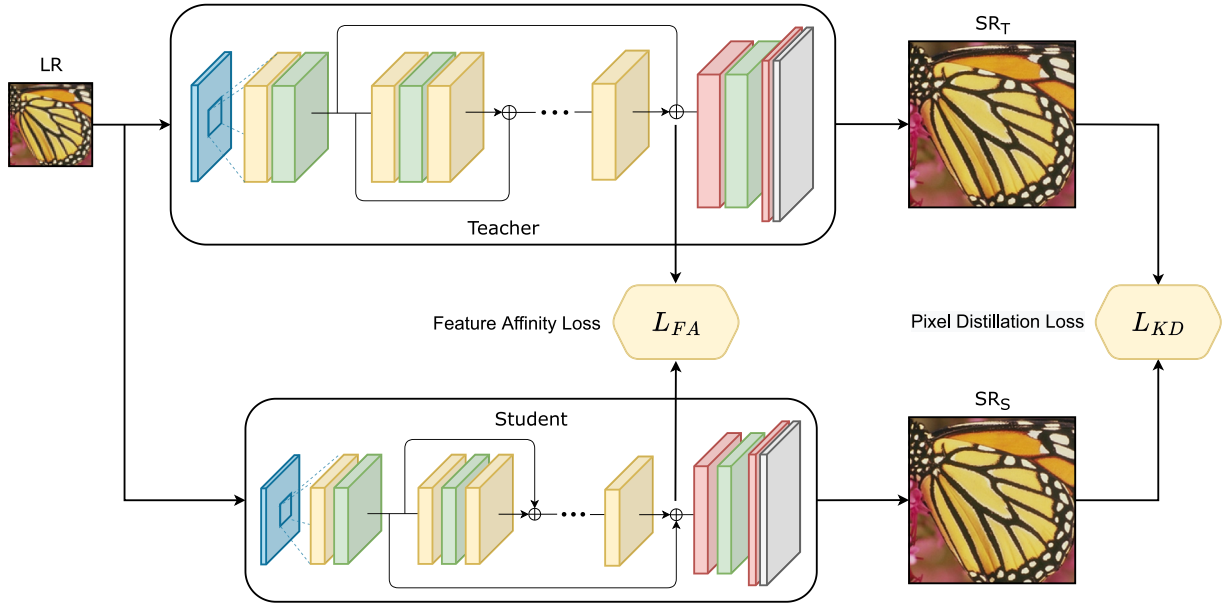


Fig. 5. EdgeSRGAN distillation process.

result obtained for different layers. These modifications experimentally lead to better training convergence. We also add another loss component, weighted by λ , which optimizes the model to generate outputs close to the teacher's ones. In our experimentation, the distillation loss is added to the overall training loss weighted by the parameter γ . The overall distillation scheme is summarized in Fig. 5.

3.4. Model interpolation

Following the procedure proposed in Wang et al. (2018b), we adopt a flexible and effective strategy to obtain a tunable trade-off between a content-oriented and GAN-trained model. This feature can be very useful for real-time applications, as it allows the SISR network to adapt to the user's needs promptly. Indeed, some real scenarios may need better perceptual quality, for example, when the remote control of a robot has to be performed by a human pilot. On the other hand, when images are used to directly feed perception, autonomous navigation, and mapping algorithms, higher pixel fidelity might be beneficial. To achieve this goal, we linearly interpolate model weights layer-by-layer, according to the following formula:

$$\theta_G^{\text{Int}} = \alpha \theta_G^{\text{PSNR}} + (1 - \alpha) \theta_G^{\text{GAN}} \quad (12)$$

where θ_G^{Interp} , θ_G^{PSNR} , and θ_G^{GAN} are the weights of the interpolated model, the PSNR model, and the GAN fine-tuned model, respectively. $\alpha \in [0, 1]$ is the interpolation weight. We report both qualitative and quantitative interpolation results for EdgeSRGAN in Section 4.3.1. We avoid the alternative technique of directly interpolating network outputs: applying this method in real time would require running two models simultaneously. Moreover, Wang et al. (2018b) report that this approach does not guarantee an optimal trade-off between noise and blur.

3.5. Model quantization

To make EdgeSRGAN achieve even lower inference latency, we apply optimization methods to the model to reduce the computational effort at the cost of a loss in performance. Several techniques have been developed to increase model efficiency in the past few years (Jacob et al., 2018), from which the employed method is chosen. We reduce the number of bits used to represent network parameters and activation functions with TFLite.² This strategy strongly increases efficiency with

² <https://www.tensorflow.org/lite/>.

Table 1

Framerate comparison of different methods for $\times 4$ and $\times 8$ upsampling, with two different input resolutions (80×60 and 160×120). The results are provided as mean and standard deviation of 10 independent experiments of 100 predictions each. Current content-oriented SISR state-of-art method SwinIR (Liang et al., 2021) is reported as a reference. Real-time and over-real-time framerates are in blue and red, respectively. The proposed solution is the only one compatible with EdgeTPU devices and allows reaching real-time performance in both conditions.

Method	Scale	Params	Framerate (80×60) [fps]		Framerate (160×120) [fps]	
			CPU	EdgeTPU	CPU	EdgeTPU
SwinIR (Liang et al., 2021)		11.9M	0.25 \pm 0.01	–	0.06 \pm 0.01	–
ESRGAN (Wang et al., 2018b)		16.7M	0.40 \pm 0.01	–	0.10 \pm 0.01	–
Real-ESRGAN (Wang et al., 2021a)		16.7M	0.44 \pm 0.01	–	0.11 \pm 0.01	–
SRGAN (Ledig et al., 2017)	$\times 4$	1.5M	2.70 \pm 0.08	–	0.95 \pm 0.02	–
AGD (Fu et al., 2020)		0.42M	3.17 \pm 0.12	–	0.88 \pm 0.01	–
EdgeSRGAN		0.66M	10.26 \pm 0.11	140.23 \pm 1.50	2.66 \pm 0.02	10.63 \pm 0.03
EdgeSRGAN-tiny		0.09M	37.99 \pm 1.42	203.16 \pm 3.03	11.76 \pm 0.20	20.57 \pm 0.05
SwinIR (Liang et al., 2021)		12.0M	0.23 \pm 0.01	–	0.06 \pm 0.01	–
EdgeSRGAN	$\times 8$	0.71M	7.70 \pm 0.31	14.26 \pm 0.06	1.81 \pm 0.04	–
EdgeSRGAN-tiny		0.11M	24.53 \pm 1.28	41.55 \pm 0.38	5.81 \pm 0.29	–

some impact on performance. We quantize weights, activations, and math operations through scale and zero-point parameters following the methodology presented by (Jacob et al., 2018):

$$r = S(q - Z) \quad (13)$$

where r is the original floating-point value, q is the quantized integer value, and S and Z are the quantization parameters (scale and zero point). A fixed-point multiplication approach is adopted to cope with the non-integer scale of S . This strategy drastically reduces memory and computational demands due to the high efficiency of integer computations on microcontrollers. For our experimentation, we deploy the quantized model on a Google Coral Edge TPU USB Accelerator.³

4. Experiments

4.1. Experimental setting

In this section, we define our method's implementation details and the procedure we followed to train and validate the efficiency of EdgeSRGAN optimally. As previously done by most GAN-based SISR works, we train the network on the high-quality DIV2K dataset (Agustsson and Timofte, 2017) with a scaling factor of 4. The dataset contains 800 training samples and 100 validation samples. We train our model with input images of size 24×24 pixels, selecting random patches from the training set. We apply data augmentation by randomly flipping or rotating the images by multiples of 90° . We adopt a batch size of 16.

For the standard EdgeSRGAN implementation, we choose $N = 8$, $F = 64$, $K = 3$, and $D = 1024$, obtaining a generator with around 660k parameters and a discriminator of over 23M (due to the fully-connected head). The discriminator is built with $F = 64$, $K = 3$, $D = 512$, and with a coefficient for LeakyReLU $\alpha = 0.2$. We first train EdgeSRGAN pixel-wise for 5×10^5 steps with Adam optimizer and a constant learning rate of 1×10^{-4} . Then, the model is fine-tuned in the adversarial setting described in Section 3 for 1×10^5 steps. Adam optimizer is used for the generator and the discriminator with a learning rate of 1×10^{-5} , further divided by 10 after 5×10^4 steps. For the loss function, we set $\xi = 1 \times 10^{-3}$ and $\eta = 0$.

To obtain an even smaller model for our distillation experiments, we build EdgeSRGAN-tiny by choosing $N = 4$, $F = 32$, and $D = 256$. We further shrink the size of the discriminator by eliminating the first compression stage ($B1$) from each block (see Fig. 3). In this configuration, we also remove the batch normalization layer from the first $B2$ block to be coherent with the larger version. The obtained generator and discriminator contain around 90k and 2.75M parameters. The pre-training procedure is the one described for EdgeSRGAN, while the adversarial training is performed with the additional distillation loss ($\gamma = 1 \times 10^{-2}$, $\lambda = 1 \times 10^{-1}$) of Eq. (11). EdgeSRGAN is used as

a teacher model, distilling its layers 2, 5, and 8 into EdgeSRGAN-tiny's layers 1, 2, and 4. The model is trained with a learning rate of 1×10^{-4} , which is further divided by 10 after 5×10^4 steps. For the loss function, we set $\xi = 1 \times 10^{-3}$ and $\eta = 0$.

Finally, we create a third version of our model to upscale images with a factor of 8. To do so, we change the first transpose convolution layer of EdgeSRGAN and EdgeSRGAN-tiny to have a stride of 4 instead of 2 and leave the rest of the architecture unchanged. The training procedure for these models is analogous to the ones used for the $\times 4$ models, with the main difference of adding a pixel-based component to the adversarial loss by posing $\eta = 1 \times 10^2$.

The optimal training hyperparameters are found by running a random search and choosing the best-performing models on DIV2K validation. During GAN training, we use PSNR to validate the models during content-based loss optimization and LPIPS (Zhang et al., 2018a) (with AlexNet backbone).

We employ TensorFlow 2 and a workstation with 64 GB of RAM, an Intel i9-12900K CPU, and an Nvidia 3090 RTX GPU to perform all the training experiments.

4.2. Real-time performance

Since the main focus of the proposed methodology is to train an optimized SISR model to be efficiently run at the edge in real time, we first report an inference speed comparison between the proposed method and other literature methodologies. All the results are shown in Table 1 as the mean and standard deviation of 10 independent experiments of 100 predictions each. We compare the proposed methodology with other GAN-based methods (Ledig et al., 2017; Wang et al., 2018b, 2021a; Fu et al., 2020) and with the current state-of-the-art in content-oriented SISR SwinIR (Liang et al., 2021). Since the original implementations of the GAN-based solutions consider $\times 4$ upsampling only, for the $\times 8$ comparison, we only report SwinIR. We select two different input resolutions for the experimentation, (80×60) and (160×120), in order to target (320×240) and (640×480) resolutions for $\times 4$ upsampling and (640×480) and (1280×960) for $\times 8$ upsampling, respectively. This choice is justified because (640×480) is a standard resolution provided by most cameras' native video stream. We also report the number of parameters for all the models.

For all the considered methods, we measure the CPU timings with the model format of the original implementation (PyTorch or TensorFlow) on a MacBook Pro with an Intel i5-8257U processor. The concept of real-time performance strongly depends on the downstream task. For robotic monitoring and teleoperation, we consider 10 fps as the minimum real-time framerate, considering over-real-time everything above 30 fps, which is the standard framerate for most commercial cameras. The proposed methodology outperforms all the other methods in inference speed and achieves real-time performance on the CPU in almost all the testing conditions. It is worth noting that AGD is

³ <https://coral.ai/>.

Table 2

Quantitative comparison of different methods for content-oriented $\times 4$ upsampling. Current SISR state-of-art method SwinIR (Liang et al., 2021) and bicubic baseline are reported as reference.

Method	Set5 (Bevilacqua et al., 2012)			Set14 (Zeyde et al., 2010)			BSD100 (Martin et al., 2001)			Manga109 (Matsui et al., 2017)			Urban100 (Huang et al., 2015)		
	PSNR \uparrow	SSIM \uparrow	LPIPS \downarrow	PSNR \uparrow	SSIM \uparrow	LPIPS \downarrow	PSNR \uparrow	SSIM \uparrow	LPIPS \downarrow	PSNR \uparrow	SSIM \uparrow	LPIPS \downarrow	PSNR \uparrow	SSIM \uparrow	LPIPS \downarrow
Bicubic	28.632	0.814	0.340	26.212	0.709	0.441	26.043	0.672	0.529	25.071	0.790	0.318	23.236	0.661	0.473
SwinIR (Liang et al., 2021)	32.719	0.902	0.168	28.939	0.791	0.268	27.834	0.746	0.358	31.678	0.923	0.094	27.072	0.816	0.193
SRGAN (Ledig et al., 2017)	32.013	0.893	0.191	28.534	0.781	0.294	27.534	0.735	0.396	30.292	0.906	0.111	25.959	0.782	0.244
ESRGAN (Wang et al., 2018b) ^a	32.730	0.901	0.181	28.997	0.792	0.275	27.838	0.745	0.371	31.644	0.920	0.097	27.028	0.815	0.201
AGD (Fu et al., 2020)	31.708	0.889	0.178	28.311	0.775	0.291	27.374	0.729	0.385	29.413	0.897	0.118	25.506	0.767	0.250
EdgeSRGAN	31.729	0.889	0.191	28.303	0.774	0.301	27.359	0.728	0.405	29.611	0.897	0.120	25.469	0.764	0.266
EdgeSRGAN-tiny	30.875	0.873	0.204	27.796	0.761	0.320	26.999	0.717	0.418	28.233	0.871	0.163	24.695	0.733	0.325

\uparrow : higher is better, \downarrow : lower is better.

^aTrained on DIV2K (Agustsson and Timofte, 2017) + Flickr2K (Timofte et al., 2017) + OST (Wang et al., 2018a).

Table 3

Quantitative comparison of different methods for visual-oriented $\times 4$ upsampling. Current SISR state-of-art method SwinIR (Liang et al., 2021) and bicubic baseline are reported as reference.

Model	Set5 (Bevilacqua et al., 2012)			Set14 (Zeyde et al., 2010)			BSD100 (Martin et al., 2001)			Manga109 (Matsui et al., 2017)			Urban100 (Huang et al., 2015)		
	PSNR \uparrow	SSIM \uparrow	LPIPS \downarrow	PSNR \uparrow	SSIM \uparrow	LPIPS \downarrow	PSNR \uparrow	SSIM \uparrow	LPIPS \downarrow	PSNR \uparrow	SSIM \uparrow	LPIPS \downarrow	PSNR \uparrow	SSIM \uparrow	LPIPS \downarrow
Bicubic	28.632	0.814	0.340	26.212	0.709	0.441	26.043	0.672	0.529	25.071	0.790	0.318	23.236	0.661	0.473
SwinIR (Liang et al., 2021)	32.719	0.902	0.168	28.939	0.791	0.268	27.834	0.746	0.358	31.678	0.923	0.094	27.072	0.816	0.193
SRGAN (Ledig et al., 2017)	29.182	0.842	0.094	26.171	0.701	0.172	25.447	0.648	0.206	27.346	0.860	0.076	24.393	0.728	0.158
ESRGAN (Wang et al., 2018b) ^a	30.459	0.852	0.083	26.283	0.698	0.139	25.288	0.649	0.168	28.478	0.860	0.065	24.350	0.733	0.125
Real-ESRGAN (Wang et al., 2021a) ^a	26.617	0.807	0.169	25.421	0.696	0.234	25.089	0.653	0.282	25.985	0.836	0.149	22.671	0.686	0.214
AGD (Fu et al., 2020)	30.432	0.861	0.097	27.276	0.739	0.160	26.219	0.688	0.214	28.163	0.870	0.076	24.732	0.743	0.170
EdgeSRGAN	29.487	0.837	0.095	26.814	0.715	0.176	25.543	0.644	0.210	27.679	0.855	0.081	24.268	0.716	0.170
EdgeSRGAN-tiny	28.074	0.803	0.146	26.001	0.702	0.242	25.526	0.658	0.292	25.655	0.804	0.140	23.332	0.672	0.269
EdgeSRGAN-tiny [*]	29.513	0.841	0.132	26.950	0.727	0.220	26.174	0.673	0.282	27.106	0.845	0.130	24.117	0.704	0.249

\uparrow : higher is better, \downarrow : lower is better.

^aTrained on DIV2K (Agustsson and Timofte, 2017) + Flickr2K (Timofte et al., 2017) + OST (Wang et al., 2018a).

Table 4

Quantitative performance of the proposed method for $\times 8$ upsampling. Current SISR state-of-art method SwinIR (Liang et al., 2021), and bicubic are reported as references. \uparrow : higher is better, \downarrow : lower is better.

Model	Set5 (Bevilacqua et al., 2012)			Set14 (Zeyde et al., 2010)			BSD100 (Martin et al., 2001)			Manga109 (Matsui et al., 2017)			Urban100 (Huang et al., 2015)		
	PSNR \uparrow	SSIM \uparrow	LPIPS \downarrow	PSNR \uparrow	SSIM \uparrow	LPIPS \downarrow	PSNR \uparrow	SSIM \uparrow	LPIPS \downarrow	PSNR \uparrow	SSIM \uparrow	LPIPS \downarrow	PSNR \uparrow	SSIM \uparrow	LPIPS \downarrow
Bicubic	24.526	0.659	0.533	23.279	0.568	0.628	23.727	0.546	0.713	21.550	0.646	0.535	20.804	0.515	0.686
SwinIR (Liang et al., 2021)	27.363	0.787	0.284	25.265	0.652	0.428	24.984	0.606	0.537	25.246	0.800	0.229	23.023	0.646	0.375
EdgeSRGAN	26.462	0.755	0.321	24.507	0.626	0.460	24.590	0.587	0.567	23.840	0.753	0.294	22.001	0.592	0.463
EdgeSRGAN-tiny	26.025	0.732	0.359	24.286	0.615	0.488	24.383	0.577	0.591	23.154	0.723	0.353	21.680	0.570	0.520
EdgeSRGAN	25.307	0.680	0.228	23.585	0.558	0.348	23.547	0.514	0.386	22.719	0.680	0.257	21.102	0.522	0.374
EdgeSRGAN-tiny	25.523	0.693	0.280	23.976	0.589	0.399	24.163	0.557	0.475	22.874	0.695	0.317	21.477	0.546	0.459

specifically designed to reduce latency for GAN-based SR and has fewer parameters than EdgeSRGAN, but it still fails at achieving real-time without a GPU.

In addition, we report the framerate of the EdgeSRGAN int8-quantized models on an EdgeTPU Coral USB Accelerator. The proposed solution is the only one compatible with such devices and allows reaching over-real-time performance for (80×60) input resolution. It must be underlined how the $\times 8$ models with (160×120) input resolution cannot target the EdgeTPU device due to memory limitations.

4.3. Super-resolution results

To present quantitative results on image super-resolution, we refer to content-oriented SR for models trained with content-based loss only and visual-oriented SR for models trained with adversarial and perceptual losses. Content-based loss (mean absolute error or mean squared error) aims to maximize PSNR and SSIM, while adversarial and perceptual losses aim to maximize visual quality. We test EdgeSRGAN models on five benchmark datasets (Set5 Bevilacqua et al., 2012, Set14 Zeyde et al., 2010, BSD100 Martin et al., 2001, Manga109 Matsui et al., 2017, and Urban100 Huang et al., 2015) measuring PSNR, SSIM, and LPIPS. We follow the standard procedure for SISR adopted in Liang et al. (2021), where the metrics are computed on the luminance channel Y of the YCbCr converted images. Also, S pixels are cropped from each image border, where S is the model scale factor.

Tables 2 and 3 show the comparison with other methods for content-oriented and visual-oriented $\times 4$ SR, respectively. We report

results of other GAN-based methodologies (Ledig et al., 2017; Wang et al., 2018b, 2021a; Fu et al., 2020) as well as the current content-oriented SOTA SwinIR (Liang et al., 2021) and bicubic baseline, as reference. Unlike what is usually found in literature, we refer to the OpenCV⁴ bicubic resize implementation instead of the one present in MATLAB. For visual-oriented SR, we also report the results of the distilled tiny model EdgeSRGAN-tiny^{*}. The proposed method reaches competitive results in all the metrics, even with some degradation for tiny models due to the considerable weight reduction. The distillation method helps EdgeSRGAN-tiny training by transferring knowledge from the standard model and decreasing the degradation due to the reduced number of parameters. Note that ESRGAN and RealESRGAN are trained on Flickr2K (Timofte et al., 2017), and OST (Wang et al., 2018a) datasets in addition to DIV2K. Table 4 reports results of the $\times 8$ models, together with SwinIR and bicubic. Also, in this case, the proposed models reach competitive results, and knowledge distillation helps to reduce performance degradation in the tiny model. As a final qualitative evaluation, Fig. 6 compares the super-resolved images obtained by EdgeSRGAN with the considered state-of-the-art solutions. Our model shows comparable results, highlighting more texture and details than networks trained with pixel loss (L_{MSE}) while remaining true to the ground truth image.

⁴ https://docs.opencv.org/2.4/modules/imgproc/doc/geometric_transformations.html#resize.

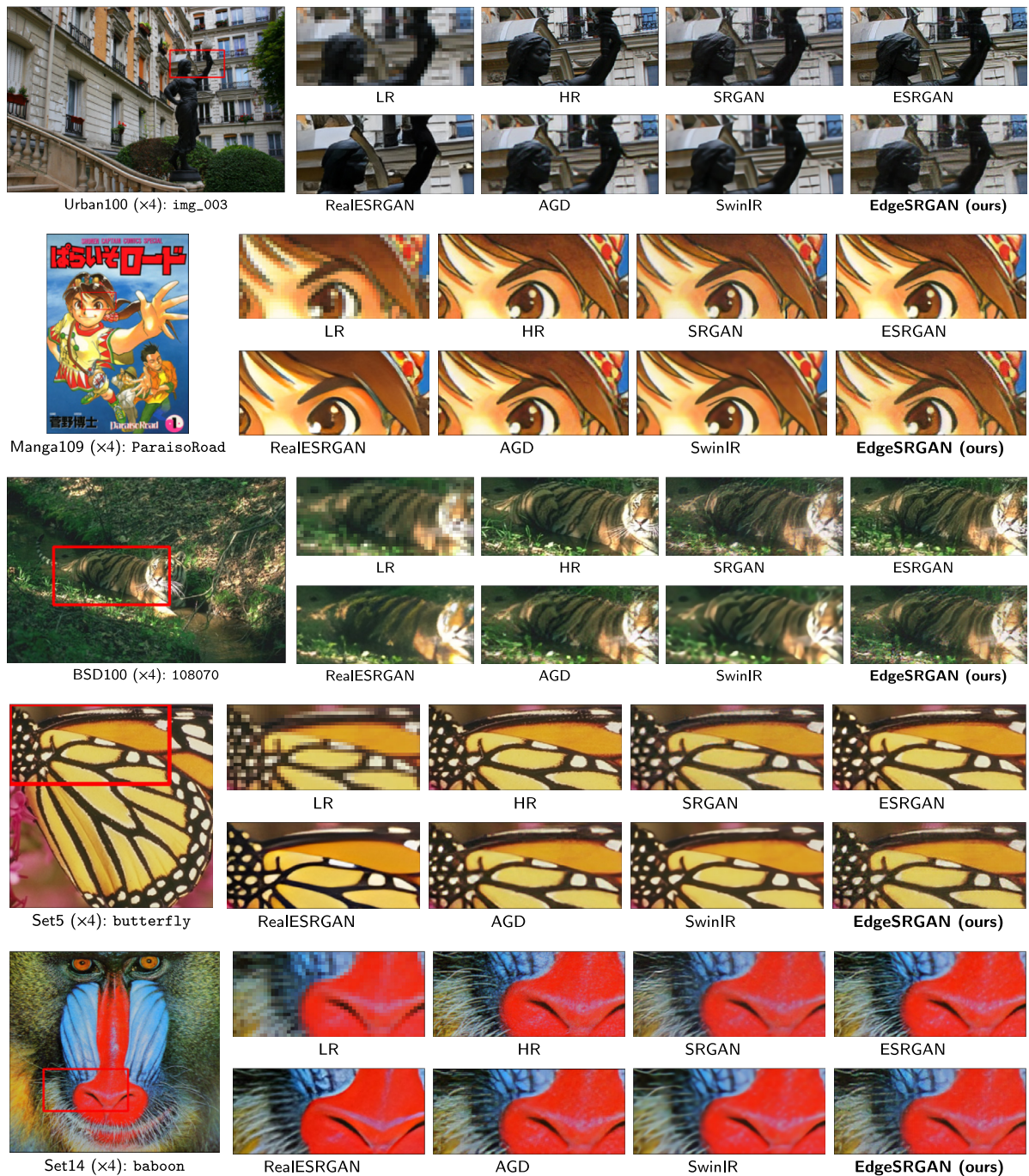


Fig. 6. Visual comparison of bicubic image SR ($\times 4$) methods on random samples from the considered datasets. EdgeSRGAN achieves results that are comparable to state-of-the-art solutions with $\sim 10\%$ of the weights (see Ledig et al., 2017; Wang et al., 2018b; Chen et al., 2022; Fu et al., 2020; Liang et al., 2021).

4.3.1. Model interpolation

We report the results of network interpolation on the benchmark datasets in Fig. 8. We consider α values between 0 and 1 with a step of 0.1, with 0 implying a full visual-oriented model and 1 a full content-oriented one. All results refer to the standard EdgeSRGAN model for $\times 4$ upsampling. This procedure effectively shows how it is possible to choose the desired trade-off between content-oriented and visual-oriented SR simply by changing the interpolation weight α . An increase in the weight value causes an improvement of the content-related metrics PSNR and SSIM and a worsening of the perceptual index LPIPS. This behavior holds for all the test datasets, validating the proposed approach. This procedure can be easily carried out in a real-time application and only requires computing the interpolated

weights once. Thus, it does not affect any way the inference speed. For an additional visual evaluation, Fig. 7 reports the outputs obtained for increasing values of α on a random dataset sample.

4.3.2. Model quantization

To target Edge TPU devices and reach over-real-time inference results, we follow the quantization scheme of Eq. (13) for both weights and activations to obtain a full-integer model. Since quantized models must have a fixed input shape, we generate a full-integer network for each input shape of the testing samples. We use the 100 images from the DIV2K validation set as a representative dataset to calibrate the quantization algorithm. We refer to the int8-quantized standard model as EdgeSRGANi8. As for the tiny model, we optimize the distilled

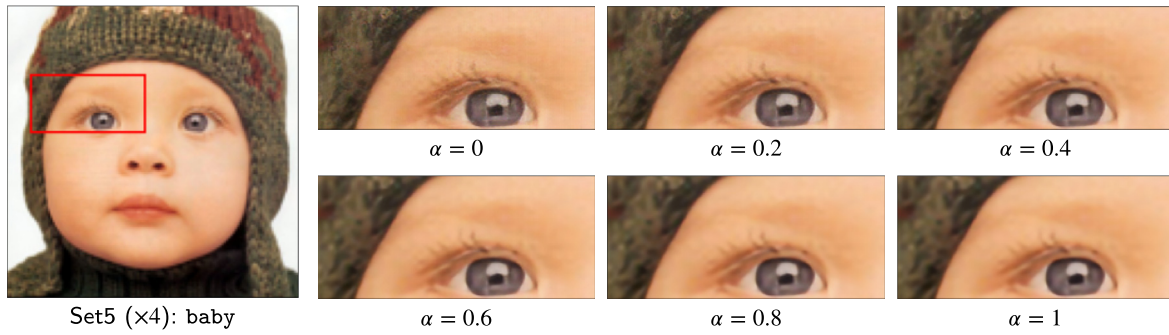


Fig. 7. Visual comparison of interpolated EdgeSRGAN for different values of α . Values closer to 1 generate outputs focused on content fidelity, while small values go towards visually pleasing results.

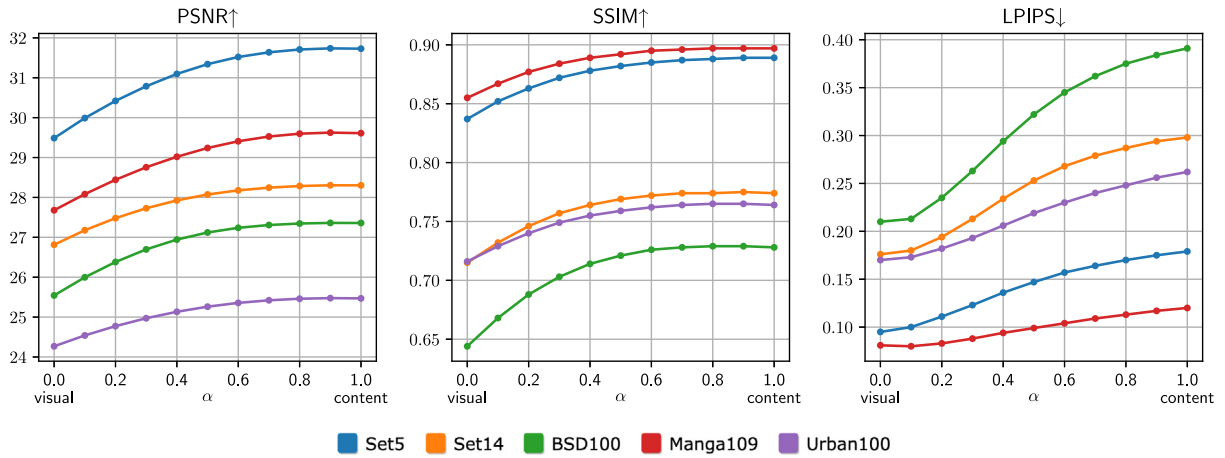


Fig. 8. EdgeSRGAN network interpolation results on the benchmark datasets for $\times 4$ upsampling. Changing the network interpolation weight α , it is possible to select the desired trade-off between content-oriented and visual-oriented SR. \uparrow : higher is better, \downarrow : lower is better.

Table 5

Quantitative performance of the full-integer quantized models for $\times 4$ and $\times 8$ visual-based SR. \uparrow : higher is better, \downarrow : lower is better.

Model	Scale	Set5 (Bevilacqua et al., 2012)			Set14 (Zeyde et al., 2010)			BSD100 (Martin et al., 2001)			Manga109 (Matsui et al., 2017)			Urban100 (Huang et al., 2015)		
		PSNR \uparrow	SSIM \uparrow	LPIPS \downarrow	PSNR \uparrow	SSIM \uparrow	LPIPS \downarrow	PSNR \uparrow	SSIM \uparrow	LPIPS \downarrow	PSNR \uparrow	SSIM \uparrow	LPIPS \downarrow	PSNR \uparrow	SSIM \uparrow	LPIPS \downarrow
EdgeSRGANi8	$\times 4$	27.186	0.721	0.209	24.714	0.475	0.342	23.675	0.484	0.438	25.601	0.712	0.221	22.802	0.580	0.341
EdgeSRGANi8-tiny \approx		27.330	0.710	0.257	24.807	0.562	0.390	23.837	0.485	0.481	25.299	0.696	0.286	22.580	0.538	0.454
EdgeSRGANi8	$\times 8$	24.433	0.602	0.312	22.846	0.477	0.440	22.609	0.422	0.492	22.227	0.603	0.342	20.525	0.433	0.499
EdgeSRGANi8-tiny		24.956	0.642	0.333	23.487	0.532	0.461	23.591	0.494	0.544	22.445	0.632	0.386	21.125	0.489	0.548

network EdgeSRGANi8-tiny \approx . Results for the visual-oriented optimized models are shown in Table 5. Due to the full-integer models' reduced activation and weight, we experience a great increase in inference speed up to over-real-time at the cost of degradation in SR performance. All the proposed quantized models still outperform the bicubic baseline on the perceptual index LPIPS and therefore represent a good option for applications in which really fast inference is needed. A comparison of different models for visual-oriented $\times 4$ upsampling is shown in Fig. 1. We consider LPIPS performance on the Set5 dataset compared to framerate.

4.4. Ablation study

To further verify the effectiveness of our model for real-time super-resolution, we conduct an ablation study to analyze the effect of our architectural design choices. In particular, we benchmark EdgeSRGAN at four progressive steps, reporting fidelity, perceptual performance, and inference speed. The steps we consider are the following:

1. Reducing the number of residual blocks N ;
2. Replacing the Pixel Shuffle upsampling stage with Transpose Convolutions;
3. Removing Batch Normalization;

4. Replacing PReLU activations with ReLU.

The last step corresponds to the final version of EdgeSRGAN. For each step of the model, we use the same training procedure described in 3.2 and measure the inference speed on the CPU at (80×60) and (160×120) input resolutions. All the results are reported in Table 6. The experimentation confirms that each compression step gains substantial inference speed by trading minimal perceptual quality. Overall, we observe -3.7% LPIPS perceptual quality and $+280\%$ inference speed.

4.5. Application: Image transmission for mobile robotics

Our real-time SISR can provide competitive advantages in a wide variety of practical engineering applications. In this section, we target a specific use case of mobile robotics, proposing our EdgeSRGAN system as an efficient deep learning-based solution for real-time image transmission. Indeed, robot remote control in unknown terrains needs a reliable transmission of visual data at a satisfying framerate, preserving robustness even in bandwidth-degraded conditions. This requirement is particularly relevant for high-speed platforms and UAVs. Dangerous or delicate tasks such as tunnel exploration, inspection, or open space missions all require an available visual stream for human supervision,

Table 6

Results of the ablation study conducted on EdgeSRGAN for four different steps. The last step corresponds to the final model. Overall, we observe -3.7% LPIPS perceptual quality and $+280\%$ inference speed. \uparrow : higher is better, \downarrow : lower is better.

Model	Params	Set5			Set14			BSD100			Manga100			Urban100			Inference Speed (fps)	
		PSNR \uparrow	SSIM \uparrow	LPIPS \downarrow	PSNR \uparrow	SSIM \uparrow	LPIPS \downarrow	PSNR \uparrow	SSIM \uparrow	LPIPS \downarrow	PSNR \uparrow	SSIM \uparrow	LPIPS \downarrow	PSNR \uparrow	SSIM \uparrow	LPIPS \downarrow	80×60	160×120
SRGAN	1.5M	29,18	0,842	0,094	26,17	0,701	0,172	25,45	0,648	0,206	27,35	0,860	0,076	24,39	0,728	0,158	2.00 ± 0.03	0.48 ± 0.01
$N = 8$	956k	29,38	0,839	0,088	26,55	0,703	0,170	25,08	0,628	0,207	27,49	0,852	0,085	24,21	0,718	0,168	2.47 ± 0.01	0.62 ± 0.01
TransposeConv	663k	28,98	0,829	0,113	26,46	0,706	0,204	25,25	0,641	0,243	26,72	0,833	0,116	23,66	0,689	0,214	9.16 ± 0.31	2.52 ± 0.03
No BatchNorm	661k	29,40	0,838	0,105	26,65	0,709	0,194	25,09	0,630	0,236	27,54	0,851	0,091	24,01	0,707	0,191	9.91 ± 0.16	2.56 ± 0.06
ReLU	661k	29,49	0,837	0,095	26,81	0,715	0,176	25,54	0,644	0,210	27,68	0,855	0,081	24,27	0,716	0,170	10.26 ± 0.11	2.66 ± 0.02

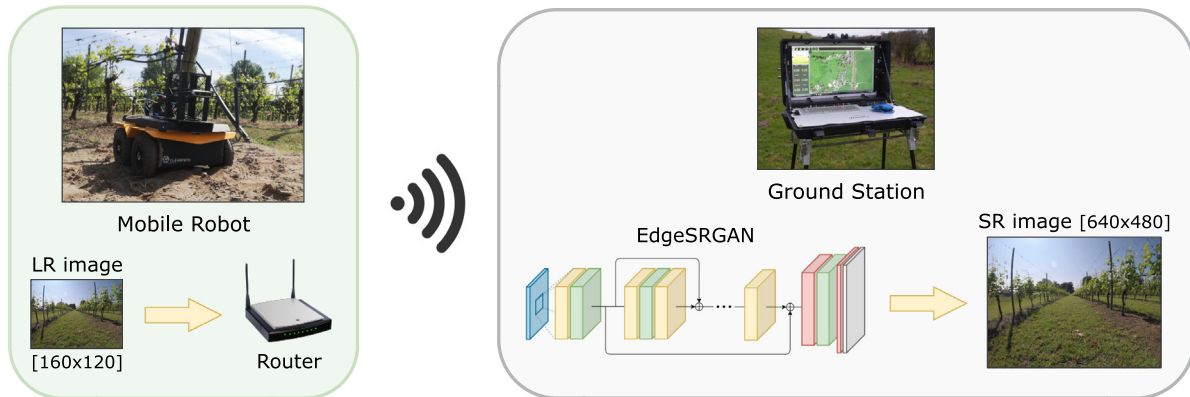


Fig. 9. Efficient image transmission system with EdgeSRGAN for mobile robotic applications in outdoor environments.

regardless of the autonomy level of the platform. In the last few years, the robotics community has focused on developing globally shared solutions for robot software and architectures and handling data communications between multiple platforms and devices. ROS2 (Macenski et al., 2022) is the standard operative system for robotic platforms. It is a middleware based on a Data Distribution System (DDS) protocol where application nodes communicate with each other through a topic with a publisher/subscriber mechanism. However, despite the most recent attempts to improve the reliability and efficiency of message and data packet communications between different nodes and platforms, heavier data transmission, such as image streaming, is not yet optimized and reliable.

The typical practical setting used for robot teleoperation and exploration in unknown environments is composed of a ground station and a rover connected to the same wireless network. As shown in Fig. 9, we adopted this ground station configuration to test the transmission of images through a ROS2 topic, as should be done in any robotic application to stream what the robot sees or to receive visual data and feed perception and control algorithms for autonomous navigation and mapping. For this experiment, we use both an Intel RealSense D435i camera⁵ and a Logitech C920 webcam⁶ mounted on a Clearpath Jackal robot,⁷ together with a Microhard BulletPlus⁸ router for image transmission. The available image resolutions with RealSense cameras, the standard RGBD sensors for visual perception in robotics, are (320×240) and (640×480) , whereas the framerate typically varies between 15 and 30 fps.

Despite the absence of strong bandwidth limitations, transmission delays, or partial loss of packets, the maximum resolution and framerate allowed by ROS2 communication are extremely low: we find that at 30 fps, the maximum transmissible resolution for RGB is (120×120) with a bandwidth of 20 Mb/s while reducing the framerate to 5 fps the limit is (320×240) . This strict trade-off between framerate

and resolution hinders the high-speed motion of a robotic platform in a mission, increasing the risk of collision due to reduced scene supervision. Even selecting *best effort* in the Quality of Service (QoS) settings, which manage the reception of packages through topics, the detected performances are always scarce.

Adopting our real-time Super-Resolution system ensures the timely arrival of RGB and depth images via ROS2. Thanks to the fast-inference performance of EdgeSRGAN, we can stream low-resolution images (80×60) at a high framerate (30 fps) and receive a high-resolution output: (320×240) with a $\times 4$ image upsampling and (640×480) with a $\times 8$ upsampling, showing a clear improvement on standard performance. Our system allows the ground station to access the streaming data through a simple ROS topic. Hence, it provides multiple competitive advantages in robotic teleoperation and autonomous navigation: high-resolution images can be directly exploited by the human operator for remote control. Moreover, they can be used to feed computationally hungry algorithms like sensorimotor agents, visual-odometry, or visual-SLAM, which we may prefer to run on the ground station to save the constrained power resources of the robot and significantly boost the autonomy level of the mission. In Fig. 10, we report a qualitative comparison to highlight the effectiveness of EdgeSRGAN for real-world robotic scenarios. In particular, we consider apple monitoring, navigation in vineyards, drone surveillance for autonomous rovers, and tunnel inspection.

We also test video transmission performance in a more general framework to reproduce all the potential bandwidth conditions. We use the well-known video streaming library GStreamer⁹ to transmit video samples changing the available bandwidth. We progressively reduce the bandwidth from 10 Mbps to 10 kbps using the Wondershaper library¹⁰ and measure the framerate at the receiver side. We use 10 s of the standard video sample *smpte* natively provided by GStreamer *videotestsrc* video source at 30 fps, and we encode it for transmission using MJPEG and H264 video compression standards. The encoding is performed offline to ensure that all the available resources are reserved for transmission only. Indeed, most cameras provide hardware-encoded

⁵ <https://www.intelrealsense.com/depth-camera-d435i/>.

⁶ <https://www.logitech.com/it-it/products/webcams/c920-pro-hd-webcam.960-001055.html>.

⁷ <https://clearpathrobotics.com/jackal-small-unmanned-ground-vehicle/>.

⁸ <https://www.microhardcorp.com/BulletPlus-NA2.php>.

⁹ <https://gstreamer.freedesktop.org/>.

¹⁰ <https://github.com/magnific0/wondershaper>.



Fig. 10. Qualitative demonstration of applying EdgeSRGAN ($\times 4$) on real scenarios (zoom for more detail). From top to bottom: apple monitoring, navigation in vineyards, drone surveillance for autonomous rovers, and tunnel inspection.

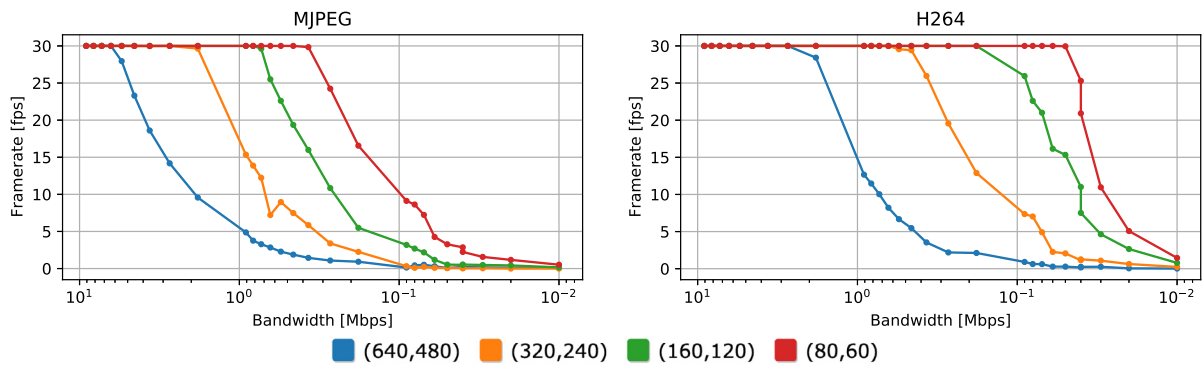


Fig. 11. Framerate results vs. bandwidth for video transmission at different input resolutions with MJPEG and H264 compression. Bandwidth is in log scale.

video sources without requiring software compression. To be consistent with the other experiments, we keep using (640×480) and (320×240) as high resolutions and (160×120) and (80×60) as low resolutions. Each experiment is performed 10 times to check the consistency in results. Fig. 11 presents the average framerate achieved with different bandwidths. Streaming video directly without any middleware, such

as ROS2, ensures a higher transmission performance. However, as expected, streaming high-resolution images is impossible in the case of low bandwidth and the framerate quickly drops to very low values, resulting unsuitable for real-time applications. On the other hand, lower resolutions can be streamed with minimal frame drop, even with lower available bandwidths. H264 compression shows the same behavior as

MJPEG but shifts to lower bandwidths. Indeed, H264 is more sophisticated and efficient, as it uses temporal frame correlation in addition to spatial compression. In a practical application with a certain bandwidth constraint, a proper combination of a low-resolution video source and an SR model can be selected to meet the desired framerate requirements on the available platform (CPU or Edge TPU). This mechanism can also be dynamically and automatically activated and deactivated depending on the current connectivity to avoid framerate drops and ensure a smooth image transmission.

5. Conclusions and future works

In this paper, we proposed a novel Edge AI model for SISR exploiting the Generative Adversarial approach. Inspired by popular state-of-the-art solutions, we design EdgeSRGAN, which obtains comparable results, being an order of magnitude smaller in terms of the number of parameters. Our model is 3 times faster than SRGAN, 30 times faster than ESRGAN, and 50 times faster than SwinIR while retaining similar or even better LPIPS performance. To gain additional inference speed, we applied knowledge distillation to EdgeSRGAN and obtained an even smaller network (EdgeSRGAN-tiny) which gains an additional 4x speed with limited performance loss. Moreover, model quantization is used to optimize the model for execution on an Edge TPU. At the same time, network interpolation was implemented to allow potential users to balance the model output between pixel-wise fidelity and perceptual quality. Extensive experimentation on several datasets confirms the effectiveness of our model regarding both performance and latency. Finally, we considered the application of our solution for robot teleoperation, highlighting the validity and robustness of EdgeSRGAN in many practical scenarios in which the transmission bandwidth is limited. Future work may investigate the effect of additional optimization techniques, such as pruning (Li et al., 2017) and neural architecture search (Pham et al., 2018). Moreover, developing optimized Edge AI versions of more recent architectures like transformers (Liang et al., 2021) might bring advantages in tackling real-time SISR.

CRedit authorship contribution statement

Simone Angarano: Conceptualization, Investigation, Methodology, Software, Writing, Revision. **Francesco Salvetti:** Conceptualization, Investigation, Software, Writing, Revision. **Mauro Martini:** Conceptualization, Investigation, Software, Writing, Revision. **Marcello Chiaberge:** Funding acquisition, Supervision, Project administration.

Declaration of competing interest

The authors declare that they have no known competing financial interests or personal relationships that could have appeared to influence the work reported in this paper.

Data availability

All the data used for our research is available as open-source datasets. The sources are referenced in the paper.

Acknowledgments

This work has been developed with the contribution of the Politecnico di Torino Interdepartmental Center for Service Robotics PIC4SeR¹¹ and SmartData@Polito.¹²

References

- Aghi, D., Cerrato, S., Mazzia, V., Chiaberge, M., 2021. Deep semantic segmentation at the edge for autonomous navigation in vineyard rows. In: 2021 IEEE/RSJ International Conference on Intelligent Robots and Systems (IROS). IEEE, pp. 3421–3428.
- Aguinaldo, A., Chiang, P.-Y., Gain, A., Patil, A., Pearson, K., Feizi, S., 2019. Compressing gans using knowledge distillation. ArXiv Preprint.
- Agustsson, E., Timofte, R., 2017. Ntire 2017 challenge on single image super-resolution: Dataset and study. In: Proceedings of the IEEE Conference on Computer Vision and Pattern Recognition Workshops. pp. 126–135.
- Almanza-Medina, J.E., Henson, B., Zakharov, Y.V., 2021. Deep learning architectures for navigation using forward looking sonar images. IEEE Access 9, 33880–33896.
- Angarano, S., Mazzia, V., Salvetti, F., Fantin, G., Chiaberge, M., 2021. Robust ultra-wideband range error mitigation with deep learning at the edge. Eng. Appl. Artif. Intell. 102, 104278.
- Bae, H., Jang, K., An, Y.-K., 2021. Deep super resolution crack network (SrcNet) for improving computer vision-based automated crack detectability in situ bridges. Struct. Health Monit. 20 (4), 1428–1442.
- Bevilacqua, M., Roumy, A., Guillemot, C., Morel, M.-L.A., 2012. Low-complexity single-image super-resolution based on nonnegative neighbor embedding. In: British Machine Vision Conference (BMVC).
- Brodie, A., Vasdev, N., 2018. The future of robotic surgery. Ann. R. Coll. Surgeons Engl. 100 (Supplement 7), 4–13.
- Cao, J., Li, Y., Zhang, K., Van Gool, L., 2021. Video super-resolution transformer. arXiv preprint arXiv:2106.06847.
- Chen, H., He, X., Qing, L., Wu, Y., Ren, C., Sheriff, R.E., Zhu, C., 2022. Real-world single image super-resolution: A brief review. Inf. Fusion 79, 124–145.
- Chen, J., Ran, X., 2019. Deep learning with edge computing: A review. Proc. IEEE 107 (8), 1655–1674.
- Chen, H., Wang, Y., Guo, T., Xu, C., Deng, Y., Liu, Z., Ma, S., Xu, C., Xu, C., Gao, W., 2021. Pre-trained image processing transformer. In: Proceedings of the IEEE/CVF Conference on Computer Vision and Pattern Recognition. pp. 12299–12310.
- Dai, T., Cai, J., Zhang, Y., Xia, S.-T., Zhang, L., 2019. Second-order attention network for single image super-resolution. In: Proceedings of the IEEE/CVF Conference on Computer Vision and Pattern Recognition. pp. 11065–11074.
- Dong, C., Loy, C.C., He, K., Tang, X., 2015. Image super-resolution using deep convolutional networks. IEEE Trans. Pattern Anal. Mach. Intell. 38 (2), 295–307.
- Drew, D.S., 2021. Multi-agent systems for search and rescue applications. Curr. Robot. Rep. 2 (2), 189–200.
- Elmokadem, T., Savkin, A.V., 2022. A method for autonomous collision-free navigation of a quadrotor UAV in unknown tunnel-like environments. Robotica 40 (4), 835–861.
- Fu, Y., Chen, W., Wang, H., Li, H., Lin, Y., Wang, Z., 2020. AutoGAN-Distiller: searching to compress generative adversarial networks. In: Proceedings of the 37th International Conference on Machine Learning. pp. 3292–3303.
- Goodfellow, I., Pouget-Abadie, J., Mirza, M., Xu, B., Warde-Farley, D., Ozair, S., Courville, A., Bengio, Y., 2014. Generative adversarial nets. Adv. Neural Inf. Process. Syst. 27.
- Gou, J., Yu, B., Maybank, S.J., Tao, D., 2021. Knowledge distillation: A survey. Int. J. Comput. Vis. 129 (6), 1789–1819.
- He, Z., Dai, T., Lu, J., Jiang, Y., Xia, S.-T., 2020. Fakd: Feature-affinity based knowledge distillation for efficient image super-resolution. In: 2020 IEEE International Conference on Image Processing (ICIP). IEEE, pp. 518–522.
- Hedayati, H., Walker, M., Szafir, D., 2018. Improving collocated robot teleoperation with augmented reality. In: Proceedings of the 2018 ACM/IEEE International Conference on Human-Robot Interaction. pp. 78–86.
- Heo, B., Kim, J., Yun, S., Park, H., Kwak, N., Choi, J.Y., 2019a. A comprehensive overhaul of feature distillation. In: Proceedings of the IEEE/CVF International Conference on Computer Vision. pp. 1921–1930.
- Heo, B., Lee, M., Yun, S., Choi, J.Y., 2019b. Knowledge transfer via distillation of activation boundaries formed by hidden neurons. In: Proceedings of the AAAI Conference on Artificial Intelligence, Vol. 33. pp. 3779–3787.
- Hinton, G., Vinyals, O., Dean, J., et al., 2015. Distilling the knowledge in a neural network. arXiv preprint arXiv:1503.02531.
- Huang, J.-B., Singh, A., Ahuja, N., 2015. Single image super-resolution from transformed self-exemplars. In: Proceedings of the IEEE Conference on Computer Vision and Pattern Recognition. pp. 5197–5206.
- Islam, M., Luo, P., Sattar, J., 2020. Simultaneous enhancement and super-resolution of underwater imagery for improved visual perception. In: Toussaint, M., Bicchi, A., Hermans, T. (Eds.), Robotics. In: Robotics: Science and Systems, MIT Press Journals.
- Jacob, B., Kligys, S., Chen, B., Zhu, M., Tang, M., Howard, A., Adam, H., Kalenichenko, D., 2018. Quantization and training of neural networks for efficient integer-arithmetic-only inference. In: Proceedings of the IEEE Conference on Computer Vision and Pattern Recognition. pp. 2704–2713.
- Kim, J., Lee, J.K., Lee, K.M., 2016. Accurate image super-resolution using very deep convolutional networks. In: Proceedings of the IEEE Conference on Computer Vision and Pattern Recognition. pp. 1646–1654.

¹¹ <https://pic4ser.polito.it>

¹² <https://smartdata.polito.it>

- Ledig, C., Theis, L., Huszár, F., Caballero, J., Cunningham, A., Acosta, A., Aitken, A., Tejani, A., Totz, J., Wang, Z., et al., 2017. Photo-realistic single image super-resolution using a generative adversarial network. In: Proceedings of the IEEE Conference on Computer Vision and Pattern Recognition. pp. 4681–4690.
- Li, H., Kadav, A., Durdanovic, I., Samet, H., Graf, H.P., 2017. Pruning filters for efficient ConvNets. In: International Conference on Learning Representations.
- Li, D., Xu, J., He, H., Wu, M., 2021. An underwater integrated navigation algorithm to deal with DVL malfunctions based on deep learning. IEEE Access 9, 82010–82020.
- Li, Y., Zhang, K., Timofte, R., Van Gool, L., Kong, F., Li, M., Liu, S., Du, Z., Liu, D., Zhou, C., et al., 2022. Ntire 2022 challenge on efficient super-resolution: Methods and results. In: Proceedings of the IEEE/CVF Conference on Computer Vision and Pattern Recognition. pp. 1062–1102.
- Liang, J., Cao, J., Sun, G., Zhang, K., Van Gool, L., Timofte, R., 2021. Swinir: Image restoration using swin transformer. In: Proceedings of the IEEE/CVF International Conference on Computer Vision. pp. 1833–1844.
- Lim, B., Son, S., Kim, H., Nah, S., Mu Lee, K., 2017. Enhanced deep residual networks for single image super-resolution. In: Proceedings of the IEEE Conference on Computer Vision and Pattern Recognition Workshops. pp. 136–144.
- Liu, D., Kong, H., Luo, X., Liu, W., Subramaniam, R., 2021. Bringing AI to edge: From deep learning's perspective. Neurocomputing.
- Liu, J., Tang, J., Wu, G., 2020. Residual feature distillation network for lightweight image super-resolution. In: European Conference on Computer Vision. Springer, pp. 41–55.
- Lluvia, I., Lazkano, E., Ansuategi, A., 2021. Active mapping and robot exploration: A survey. Sensors 21 (7), 2445.
- Macenski, S., Foote, T., Gerkey, B., Lalancette, C., Woodall, W., 2022. Robot operating system 2: Design, architecture, and uses in the wild. Science Robotics 7 (66), eabm6074.
- Martin, D., Fowlkes, C., Tal, D., Malik, J., 2001. A database of human segmented natural images and its application to evaluating segmentation algorithms and measuring ecological statistics. In: Proceedings Eighth IEEE International Conference on Computer Vision. ICCV 2001, Vol. 2. IEEE, pp. 416–423.
- Martinez, D.E., Meinhold, W., Oshinski, J., Hu, A.-P., Ueda, J., 2021. Super resolution for improved positioning of an MRI-guided spinal cellular injection robot. J. Med. Robot. Res. 6 (01n02), 2140002.
- Martini, M., Cerrato, S., Salvetti, F., Angarano, S., Chiaberge, M., 2022. Position-agnostic autonomous navigation in vineyards with deep reinforcement learning. ArXiv Preprint.
- Matsui, Y., Ito, K., Aramaki, Y., Fujimoto, A., Ogawa, T., Yamasaki, T., Aizawa, K., 2017. Sketch-based manga retrieval using manga109 dataset. Multimedia Tools Appl. 76 (20), 21811–21838.
- Micheline, P.N., Lu, Y., Jiang, X., 2022. Edge-SR: Super-resolution for the masses. In: Proceedings of the IEEE/CVF Winter Conference on Applications of Computer Vision. pp. 1078–1087.
- Niu, B., Wen, W., Ren, W., Zhang, X., Yang, L., Wang, S., Zhang, K., Cao, X., Shen, H., 2020. Single image super-resolution via a holistic attention network. In: European Conference on Computer Vision. Springer, pp. 191–207.
- Odena, A., Dumoulin, V., Olah, C., 2016. Deconvolution and checkerboard artifacts. Distill.
- Ooyama, S., Lu, H., Kamiya, T., Serikawa, S., 2021. Underwater image super-resolution using SRCNN. In: International Symposium on Artificial Intelligence and Robotics 2021, Vol. 11884. SPIE, pp. 177–182.
- Pham, H., Guan, M., Zoph, B., Le, Q., Dean, J., 2018. Efficient neural architecture search via parameters sharing. In: International Conference on Machine Learning. PMLR, pp. 4095–4104.
- de Queiroz Mendes, R., Ribeiro, E.G., dos Santos Rosa, N., Grassi Jr., V., 2021. On deep learning techniques to boost monocular depth estimation for autonomous navigation. Robot. Auton. Syst. 136, 103701.
- Romero, A., Ballas, N., Kahou, S.E., Chassang, A., Gatta, C., Bengio, Y., 2014. Fitnets: Hints for thin deep nets. ArXiv Preprint.
- Rouček, T., Pecka, M., Čížek, P., Petříček, T., Bayer, J., Šalanský, V., Heřt, D., Petrлік, M., Báča, T., Spurný, V., et al., 2019. Darpa subterranean challenge: Multi-robotic exploration of underground environments. In: International Conference on Modelling and Simulation for Autonomous Systems. Springer, pp. 274–290.
- Roy, P., Chowdhury, C., 2021. A survey of machine learning techniques for indoor localization and navigation systems. J. Intell. Robot. Syst. 101 (3), 1–34.
- Sajjadi, M.S., Scholkopf, B., Hirsch, M., 2017. Enhancenet: Single image super-resolution through automated texture synthesis. In: Proceedings of the IEEE International Conference on Computer Vision. pp. 4491–4500.
- Shi, W., Caballero, J., Huszar, F., Totz, J., Aitken, A.P., Bishop, R., Rueckert, D., Wang, Z., 2016. Real-time single image and video super-resolution using an efficient sub-pixel convolutional neural network. In: Proceedings of the IEEE Conference on Computer Vision and Pattern Recognition (CVPR).
- Simonyan, K., Zisserman, A., 2015. Very deep convolutional networks for large-scale image recognition. In: Bengio, Y., LeCun, Y. (Eds.), 3rd International Conference on Learning Representations, ICLR 2015, San Diego, CA, USA, May 7–9, 2015, Conference Track Proceedings.
- Stotko, P., Krumpal, S., Schwarz, M., Lenz, C., Behnke, S., Klein, R., Weinmann, M., 2019. A VR system for immersive teleoperation and live exploration with a mobile robot. In: 2019 IEEE/RSJ International Conference on Intelligent Robots and Systems (IROS). pp. 3630–3637.
- Tardioli, D., Riazuelo, L., Sicignano, D., Rizzo, C., Lera, F., Villarreal, J.L., Montano, L., 2019. Ground robotics in tunnels: Keys and lessons learned after 10 years of research and experiments. J. Field Robotics 36 (6), 1074–1101.
- Timofte, R., Agustsson, E., Van Gool, L., Yang, M.-H., Zhang, L., 2017. Ntire 2017 challenge on single image super-resolution: Methods and results. In: Proceedings of the IEEE Conference on Computer Vision and Pattern Recognition Workshops. pp. 114–125.
- Wang, X., Xie, L., Dong, C., Shan, Y., 2021a. Real-esrgan: Training real-world blind super-resolution with pure synthetic data. In: Proceedings of the IEEE/CVF International Conference on Computer Vision. pp. 1905–1914.
- Wang, X., Yu, K., Dong, C., Loy, C.C., 2018a. Recovering realistic texture in image super-resolution by deep spatial feature transform. In: Proceedings of the IEEE Conference on Computer Vision and Pattern Recognition. pp. 606–615.
- Wang, X., Yu, K., Wu, S., Gu, J., Liu, Y., Dong, C., Qiao, Y., Loy, C.C., 2018b. ESRGAN: Enhanced super-resolution generative adversarial networks. In: The European Conference on Computer Vision Workshops (ECCVW).
- Wang, R., Zhang, D., Li, Q., Zhou, X.-Y., Lo, B., 2021b. Real-time surgical environment enhancement for robot-assisted minimally invasive surgery based on super-resolution. In: 2021 IEEE International Conference on Robotics and Automation (ICRA). IEEE, pp. 3434–3440.
- Xiao, X., Liu, B., Warnell, G., Stone, P., 2022. Motion planning and control for mobile robot navigation using machine learning: a survey. Auton. Robots 1–29.
- Yin, F., 2021. Inspection robot for submarine pipeline based on machine vision. In: Journal of Physics: Conference Series, Vol. 1952. IOP Publishing, 022034.
- Yuan, C., Xiong, B., Li, X., Sang, X., Kong, Q., 2022. A novel intelligent inspection robot with deep stereo vision for three-dimensional concrete damage detection and quantification. Struct. Health Monit. 21 (3), 788–802.
- Zagoruyko, S., Komodakis, N., 2016. Paying more attention to attention: Improving the performance of convolutional neural networks via attention transfer. ArXiv Preprint.
- Zein, M.K., Al Awar, M., Asmar, D., Elhadj, I.H., 2021. Deep learning and mixed reality to autocomplete teleoperation. In: 2021 IEEE International Conference on Robotics and Automation (ICRA). IEEE, pp. 4523–4529.
- Zeyde, R., Elad, M., Protter, M., 2010. On single image scale-up using sparse-representations. In: International Conference on Curves and Surfaces. Springer, pp. 711–730.
- Zhang, Y., Chen, H., Chen, X., Deng, Y., Xu, C., Wang, Y., 2021. Data-free knowledge distillation for image super-resolution. In: Proceedings of the IEEE/CVF Conference on Computer Vision and Pattern Recognition. pp. 7852–7861.
- Zhang, R., Isola, P., Efros, A.A., Shechtman, E., Wang, O., 2018a. The unreasonable effectiveness of deep features as a perceptual metric. In: Proceedings of the IEEE Conference on Computer Vision and Pattern Recognition. pp. 586–595.
- Zhang, Y., Li, K., Li, K., Wang, L., Zhong, B., Fu, Y., 2018b. Image super-resolution using very deep residual channel attention networks. In: Proceedings of the European Conference on Computer Vision (ECCV). pp. 286–301.
- Zhang, Y., Tian, Y., Kong, Y., Zhong, B., Fu, Y., 2018c. Residual dense network for image super-resolution. In: Proceedings of the IEEE Conference on Computer Vision and Pattern Recognition. pp. 2472–2481.
- Zhao, H., Gallo, O., Frosio, I., Kautz, J., 2016. Loss functions for image restoration with neural networks. IEEE Trans. Comput. Imaging 3 (1), 47–57.
- Zhu, F., Zhu, Y., Lee, V., Liang, X., Chang, X., 2021. Deep learning for embodied vision navigation: A survey. ArXiv Preprint.



Simone Angarano is a Ph.D. student in Electrical, Electronics, and Communications Engineering and a member of the Interdepartmental Center for Service Robotics at Politecnico di Torino (<https://pic4ser.polito.it/>). At the same university, he achieved a Bachelor's Degree in Electronic Engineering in 2018 and a Master's Degree in Mechatronic Engineering in 2020, presenting the thesis "Deep Learning Methodologies for UWB Ranging Error Compensation". His research focuses on Deep Learning for robotic applications, spanning computer vision, navigation, and control. His work also gives particular attention to model optimization for real-time applications and edge AI.



Francesco Salvetti is currently a Ph.D. student in Electrical, Electronics, and Communications Engineering in collaboration with the interdepartmental centers PIC4SeR (<https://pic4ser.polito.it/>) and Smart Data (<https://smartdata.polito.it/>) at Politecnico di Torino, Italy. He received his Bachelor's Degree in Electronic Engineering in 2017 and his Master's Degree in Mechatronic Engineering in 2019 at Politecnico di Torino. He is currently working on Machine Learning applied to Computer Vision and Image Processing in robotics applications.



Mauro Martini is a Ph.D. student in Electrical, Electronics, and Communication Engineering at Politecnico di Torino. He received from the Politecnico di Torino a Master's Degree with Laude in Mechatronic Engineering in 2020, with the thesis "Visual-based local motion planner with Deep Reinforcement Learning". He is now doing his research in collaboration with the Interdepartmental Center for Service Robotics (PIC4SeR, <https://pic4ser.polito.it/>). His research interests currently involve machine learning for autonomous navigation in service robotics, with a particular focus on perception and deep reinforcement learning-based planners.



Marcello Chiaberge is currently an Associate Professor within the Department of Electronics and Telecommunications, Politecnico di Torino, Turin, Italy. He is also the Co-Director of the Mechatronics Lab, Politecnico di Torino (www.lim.polito.it), Turin, and the Director and the Principal Investigator of the Interdepartmental Center for Service Robotics (PIC4SeR, <https://pic4ser.polito.it/>), Turin. He has authored more than 100 articles accepted in international conferences and journals and is the co-author of nine international patents. His research interests include the hardware implementation of neural networks and fuzzy systems and the design and implementation of reconfigurable real-time computing architectures.